Journal of Photochemistry & Photobiology, A: Chemistry 436 (2023) 114373

Contents lists available at ScienceDirect

Journal of Photochemistry & Photobiology, A: Chemistry

journal homepage: www.elsevier.com/locate/jphotochem

The role of predissociation states in the UV photooxidation of acetylene

Panagiotis Kalaitzis, Dimitris Sofikitis *, Constantine Kosmidis

Department of Physics, Atomic and Molecular Physics Laboratory, University of Ioannina, University Campus, Ioannina, GR-45110, Greece

ARTICLE INFO

MSC:
00-01
81V55

Keywords:
Photooxidation
Acetylene
Glyoxal
Rydberg states

ABSTRACT

We study the photo-induced oxidation of acetylene in two different spectral areas, around 220 and 320 nm. In both spectral areas, the dominant reaction pathways involve the rupture of the acetylene $C-H$ bond, thus primarily generating C_2H and H fragments. The released fragments react in O_2 presence resulting in glyoxal and other molecular species formation. We observe strong variations in the photooxidation rates, which point to the increased participation of excited, predissociation states, in the oxidation process. Such effects of increased excited state participation in photooxidation should be observed in a variety of photo-induced reactions, affecting the reaction spectral response and eventually the reaction cycles in terrestrial or planetary environments.

1. Introduction

The acetylene molecule is the simplest unsaturated hydrocarbon, and it is abundant in the interstellar medium as well as in planetary atmospheres. Due to its abundance and characteristic spectral features, observations of acetylene offer a major diagnostic used for the study of the atmospheric chemistry in planets and moons in our solar system [1–3]. Moreover, acetylene has a rich chemistry and, along with the ethynyl radical, can be important in hydrocarbon combustion and soot formation [4].

The acetylene oxidation reaction generates a variety of products, such as glyoxal, formic acid, formaldehyde, carbon monoxide, carbon dioxide, hydrogen and water [5]. Among these various products, glyoxal is of particular interest. It is a Volatile Organic Compound (VOC) that can be detected remotely, and due to its limited lifetime in the atmosphere, can be used as a probe of the local photochemical activity [6,7]. In particular, glyoxal formation from acetylene oxidation accounts for nearly 20% of the glyoxal found in the atmosphere [8]. Moreover, recent studies indicate that the origin of enhanced glyoxal concentration over equatorial oceans remains unclear [7].

In this work, we study the rate of glyoxal formation due to acetylene photooxidation, in acetylene/oxygen mixtures in room temperature, using tunable laser UV radiation. Previous studies which used either thermal UV sources [9] or non-tunable excimer laser radiation [10,11], could not offer information about how discrete excited states affect the photooxidation reaction. We are able to identify two different photooxidation pathways, related to excitation of either the $\tilde{A}^1A_u$ first excited state or the $3p^1\Pi$ Rydberg states [12]. The latter state, with an excitation energy that lies in the VUV region, is reached via a two-photon absorption process, and it is a fast predissociation state, a fact that prohibits its detection in multiphoton ionization experiments. Thus, our work demonstrates the importance of highly-excited Rydberg states, which even if being 'silent' in typical photoionization experiments, can have an important role in the photochemistry of acetylene. Finally, excited state participation in various photo-induced reactions, would affect the reaction spectral behavior and could be of use in the rationalization of observed VOC planetary budgets and astrochemical observations.

2. Experimental

The experimental setup is shown in Fig. 1. Tunable radiation at 440 and 640 nm was generated using a Lambda Physik Scanmate laser. The laser frequency was doubled using either a BBO (used around 440 nm) or a KDP (used around 640 nm) crystal. The output of the doubling crystals is filtered using a UG5 filter and enters the fused silica cell, after passing through an (×1/3) optical telescope, through the hole of a parabolic mirror (Thorlabs MPO249H-P01). The light coming from the broadband light source (Thorlabs SLS201 L/M), used to record the absorption spectra, is focused by the parabolic mirror into the fused silica cell. Both the broadband and the UV laser radiation exit the fused silica cell; the UV radiation is filtered out using a UV absorber and the broadband radiation, which transmits through the filter, is focused on the input of a spectrometer (Andor Shamrock SR-301-iB, utilizing a Newton EM CCD camera). The acetylene and oxygen gases are commercially obtained (Air Liquide, purity > 99.6%).

* Corresponding author.
E-mail address: sofdim@uoi.gr (D. Sofikitis).

https://doi.org/10.1016/j.jphotochem.2022.114373
Received 28 July 2022; Received in revised form 19 October 2022; Accepted 25 October 2022
Available online 4 November 2022

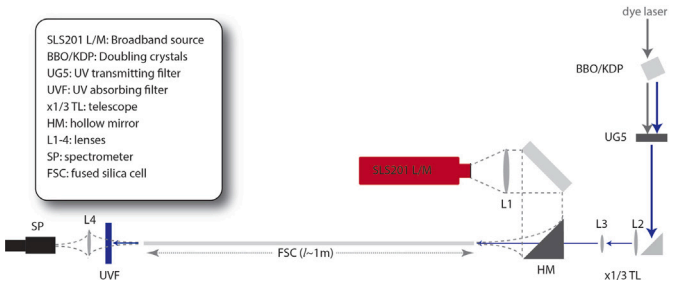

Fig. 1. Experimental set-up used for the study of acetylene photo-oxidation.

3. Results

When irradiating an acetylene/oxygen mixture with radiation around 220 nm or 320 nm, light-induced photooxidation initiates a series of reactions. Starting with the production of glyoxal from the reaction of acetylene and oxygen, a reaction branch which emanates from glyoxal oxidation, leads, through the course of at least eight more reactions, towards termination and the production of stable products [5]. Among the various products, we can monitor the initial product glyoxal (and to a lesser extend formaldehyde), through its characteristic absorption spectrum around 440 nm. A typical glyoxal absorption spectrum is shown in Fig. 2a.

The acetylene/oxygen mixture typically contains 350 Torr of O_2 and 500 Torr of C_2H_2. In Fig. 2b, a study of the glyoxal yield dependence on the acetylene/oxygen mixing ratio is shown. The glyoxal yield increases fast as the mixing ratio increases up to 0.2, while it saturates afterwards. In the experiments described hereinafter, we use an acetylene/oxygen mixing ratio close to 0.75, so that any effects related to the glyoxal production dependence on the acetylene/oxygen mixing ratio are minimized.

The initial increase of glyoxal absorption can be fitted with a simple formula $A(t) = A_{max}(1 - e^{-t/\tau})$, with A being the time-dependent absorption, A_{max} its maximum value, and τ the characteristic time constant to be extracted. Such a fit is shown in Fig. 2c. The inverse of τ gives the glyoxal production rate k_{pr} minus the destruction rate k_{des}. The glyoxal destruction rate depends on several parameters, such as glyoxal oxidation [13,14], photolysis [15] and more [13].

We can monitor the evolution of the glyoxal production time constant τ, as a function of the photon energy of the UV pulses used for the photooxidation. Fig. 3a, shows the evolution of τ with respect to the photon energy ranging from ~5.55 to ~5.75 eV. The dots correspond to the experimentally determined τ extracted using the method described in Fig. 2c. The error bars extracted from the fit have been multiplied with a factor of 10 to facilitate visibility. The pulse energy is kept around 7 μJ, however, fluctuations of the energy output of the laser between the experimental runs, as well as within each experimental run, could not be avoided, leading to an overall scatter in the measurements. However, a decreasing trend of the glyoxal production time τ with increasing photon energy is evident.

The red solid line shows a linear fit of these data, while the dashed red curves show the 99% confidence interval of this fit. If we extrapolate the linear fit towards $\tau \to 0$, it intercepts the photon energy axis in the value 5.73 eV, while the 99% confidence curves intercept the axis at 5.71 eV and 5.81 eV respectively. The D_0 (HCC-H) dissociation limit for acetylene, lies around this area and corresponds to the production of $C_2H(\tilde{X}^2\Sigma^+)$ and H (1s) fragments. In Fig. 3b, we compare the point of interception of our linear fit with the photon energy axis to the D_0 values given in Refs. [16,17]. In Fig. 3c, the evolution of the characteristic time τ as a function of the two-photon energy between 7.6 eV and 8.3 eV is shown. The pulse energy is kept around 200 μJ between the experimental runs. Similarly to Fig. 3a, the black dots correspond to the experimentally determined τ, the red solid line to the linear fit and the red dashed curves to the 99% confidence interval.

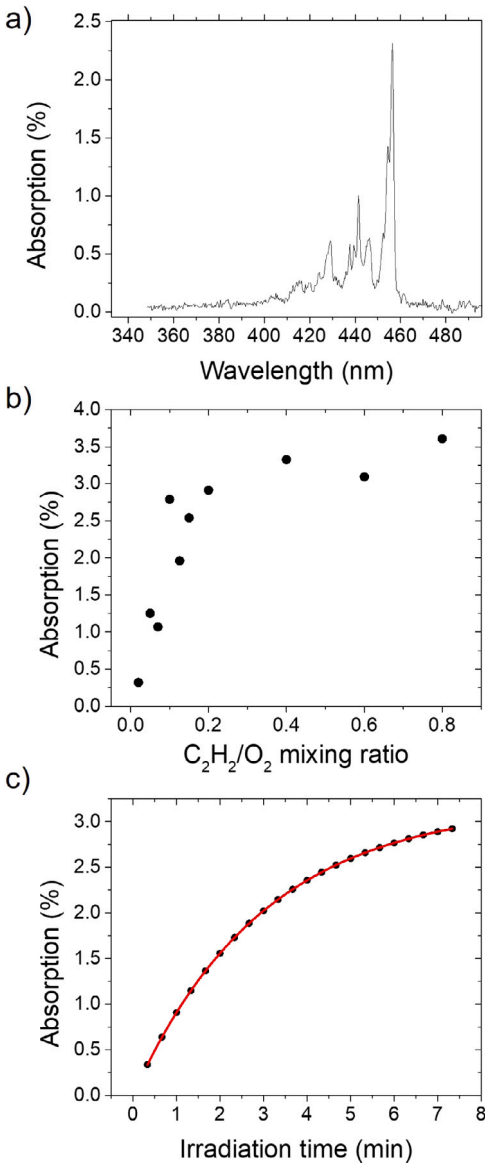

Fig. 2. (a) Glyoxal absorption spectrum recorded around 440 nm (b) Glyoxal absorption as a function of the acetylene/oxygen mixing ratio (c) Glyoxal absorption increase during the first minutes of irradiation and fit.

Fig. 3d, shows the point of interception of the linear fit shown in Fig. 3c with the photon energy axis, with the error bars corresponding to the 99% confidence intervals shown in Fig. 3c. We compare to the $3p^1\Pi_g$ state energy predicted in Ref. [12] (red dashed curve), as well as to $\tilde{C}^1\Pi_u$ state, also predicted in [12] and observed in [18], for reasons which will be made clear in the discussion.

Considering two photon excitation can be easily justified by measuring the glyoxal production rates as a function of pulse energy. Such a study of acetylene photooxidation at ~320 nm, is shown in Fig. 4, along with a fit with the function $k(E) = E^n + B$, with k being the rate, E being the pulse energy, n is a free parameter and B is an offset we introduce to account for small experimental errors. The fitting results are $B = 0.21 \pm 2.32$ and $n = 2.27 \pm 0.051$, a value which reveals the non-linear nature of the process.

4. Discussion

In Fig. 3a and c, it is clear that the photooxidation of acetylene accelerates in the vicinity of dissociating states. Acetylene photoexcitation in the wavelengths around 220 nm proceeds through the well

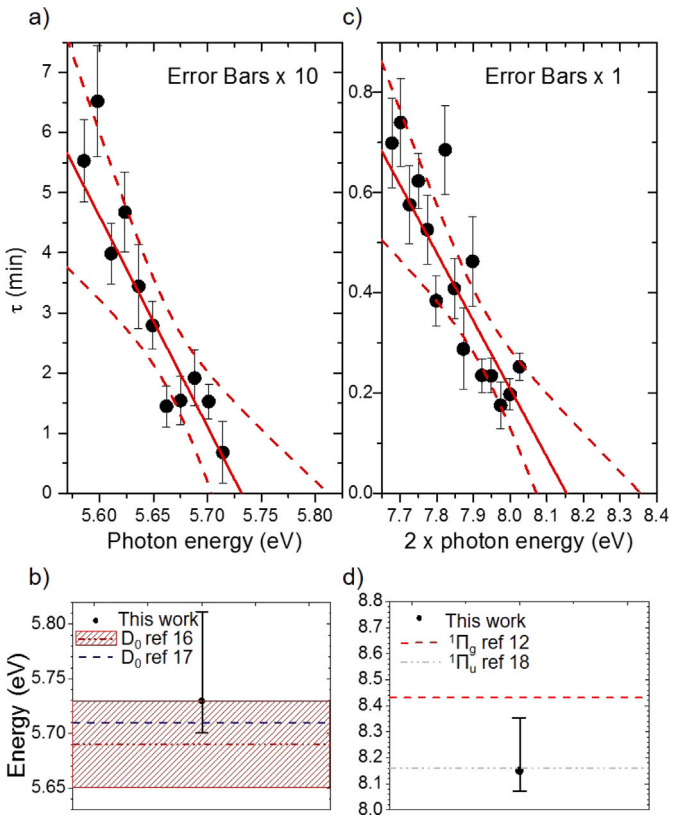

Fig. 3. (a) Evolution of the glyoxal production time as a function of the photon energy between 5.55 and 5.77 eV. The black dots correspond to our measurements, the red solid line to a linear fit and the red dashed curves indicate the 99% confidence interval (b) The point of interception of the linear fit shown in (a) compared to the D_0(HCC-H) dissociation limit of acetylene given in the references indicated in the legend. Error bars correspond to the 99% confidence intervals shown in (a). (c) Evolution of the glyoxal production time as a function of the two-photon energy between 7.7 and 8.1 eV. Again, the black dots correspond to our measurements, the red solid line to a linear fit and the red dashed curves indicate the 99% confidence interval. (d) The point of interception of the linear fit shown in (c) compared to the energies of the predissociation states given in the references indicated in the legend. Error bars correspond to the 99% confidence intervals shown in (c).

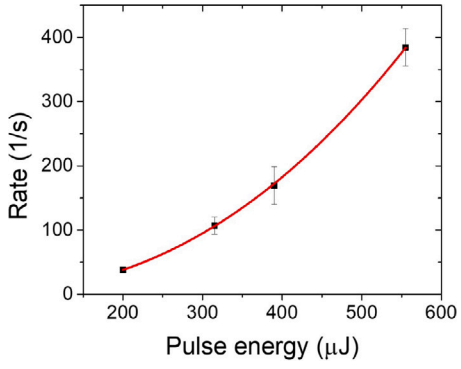

Fig. 4. Dependence of the glyoxal production rate after excitation at ~320 nm on the pulse energy and fit with a nearly quadratic function.

known $\tilde{X}^1\Sigma_g^+ - \tilde{A}^1A_u$ band [19]. While the ground $^1\Sigma_g^+$ state is of a linear geometry, the ^1A_u valence excited state is of a trans-bend geometry resulting to a long-progression of the system in the v_3' trans-bending mode, as well as in combination modes [3,17,20]. Highly excited vibrational levels in the $^1\Sigma_g^+$ ground state can be populated via subsequent radiationless deactivation processes. These processes are fast (hundreds of fs) and can take place within the duration of the pulses used in our experiments (~5 ns). The resulting vibrational distribution will thus differ from the Boltzmann distribution corresponding to thermal equilibrium. We note that, due to the large absorption cross section of acetylene in the NIR region ($>10^{-18}$ cm^2 at 1500 nm), vibrational excitation can also occur in the atmosphere, since the solar content in this region is substantial [21]. These effects lead to the appearance of hot-bands in the absorption spectrum, which are often superimposed leading to the observation of absorption continua [3]. These vibrationally excited molecules can be excited further and reach the ^1A_u or $^1\Pi_{u,g}$ states, using UV photons with energies which are marginally smaller than the energy difference between these states and the absolute ground state.

In the case of two-photon excitation around 320 nm, a similar acceleration of the photooxidation reaction is observed, converging to a two-photon energy of ~8.15 eV, as shown in Fig. 3c. At this area, a complex of Rydberg states of n = 3 is expected, among which the $3p^1\Pi_g$ state at 8.43 eV, predicted in Ref. [12]. The rich Rydberg structure of acetylene has been the subject of various experimental studies, mainly utilizing multi-photon ionization schemes [22,23], or UV-induced fluorescence spectroscopy [24,25]. In general, Rydberg states are characterized by a long lifetime, however it is known that are sensitive to surrounding pressure. Thus, under the present experimental conditions, it is expected that their lifetime will decrease. Moreover, in this energy region, some of the Rydberg states n = 3 and n = 4 series undergo rapid predissociation, a fact which prevents their detection by two color REMPI experiments [12]. Such states can be detected by probing the dissociation fragments, as is done for states in the n = 4 manifold in Refs. [26]. To the best of our knowledge, the observation of the $3p^1\Pi_g$ state has not been reported in an experimental study.

The effect of vibrational excitation leading to hot-bands in the room temperature absorption spectra [3], should be taken into consideration in the analysis of the ~320 nm two-photon excitation as well. Moreover, the low-lying ungerade C–H bend mode at 730 cm^{-1} is expected to participate to the reaction. This forces consideration of the $\tilde{C}^1\Pi_u$ Rydberg excitation, which is otherwise inaccessible from the ground state with a two-photon process, shown in Fig. 3d. The $\tilde{C}^1\Pi_u$ Rydberg state has been observed to be a strongly predissociative state as well, with a predissociation lifetime close to 50 fs [18].

It is clear that acetylene excitation into dissociating and predissociating states leads to increased photooxidation rates. Dissociation around 5.7 eV results to C-H bond rupture and thus to the production of C_2H and H fragments [27,28], and the same is to be expected upon excitation around 8.1 eV [18,29]. On the contrary, the threshold for the formation of C_2 and H_2 fragments is estimated to be around 9.24 eV^{-1} [30], and thus, this photodissociation pathway is not expected to contribute to the photooxidation processes reported in this study, neither around 220 nm nor around 320 nm. Thus, we conclude that the oxidation reactions observed here, mainly proceed following C_2H–H fragmentation of the parent C_2H_2 molecule.

An important difference between the excitation around 5.7 and 8,1 eV, is the electronic state of the C_2H fragment. For excitation around 5.7 eV, it is expected to be (predominately) the $\tilde{X}^2\Sigma^+$ ground state, while around 8.1 eV the $\tilde{A}^2\Pi$ state [17,18]. As depicted in Fig. 5, excitation around 220 nm populates the ^1A_u state and subsequently, population can be transferred via intersystem crossing to the lowest triplet state $^3B_2$, which correlates to $C_2H(\tilde{X})$ and $H(1s)$ products. When two-photon excitation at 304 nm is considered, acetylene molecules are excited to the $^1\Pi_{u,g}$ states. These states preserve their Rydberg character within the Franck–Condon region, but acquire σ^* anti-bonding character at later times, as the C–H bond length increases [31]. At large C–H bond distances, predissociation proceeds via crossing with the $\pi\sigma^*$ states, which leads to the production of $C_2H(\tilde{A})$ and $H(1s)$ fragments.

The energetic difference between these two states of the C_2H fragment, is close to 0.47 eV [32], and it is the main difference in the products between those two dissociation pathways, since any differences in the translational kinetic energies of the C_2H fragment should

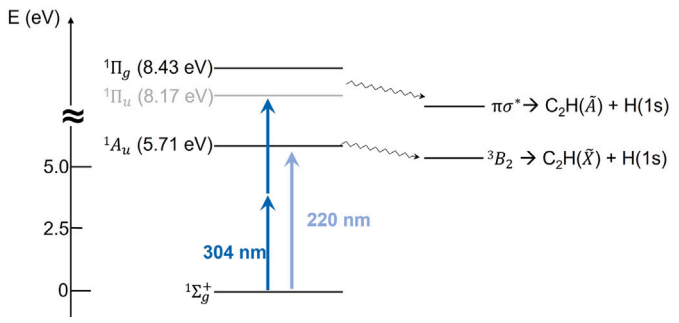

Fig. 5. Simplified diagram of the acetylene states involved in the experiment.

be minuscule, due to the large mass difference between the C_2H and H fragments. It is difficult to directly compare the rates of the photooxidation reaction in the two spectral areas studied, i.e. near 220 and 320 nm, since the laser intensities and excitation probabilities differ. However, we expect that the electronically excited C_2H fragments produced predominately after excitation around 320 nm, should lead to increased reaction rates, since reaction pathways which are endothermic when C_2H is in the ground electronic state $\tilde{X}$, become exothermic when the first excited $\tilde{A}$ state is considered [32].

An additional question is whether high electronic excitation of the C_2H_2 in an oxygen rich environment, can also accelerate photooxidation, in the absence of fragmentation. In our experiments, only the $\tilde{A}^1A_u$ valence excited state and the $\tilde{C}^1\Pi$ Rydberg states, all strongly dissociating states, are within reach. Additionally, in a collision-rich environment of a C_2H_2–O_2 thermal sample such as the ones used here, several characteristics of Rydberg excited states, such as the long lifetime for example, would be severely hindered. However, we are currently underway to designing experiments which would examine the role of non-dissociating acetylene excited states in the photooxidation reaction.

The acceleration of the photooxidation reaction after excitation in the vicinity of Rydberg dissociating states, should be a general characteristic of many photo-induced reactions. Variations of the reaction rates around resonances, such as the ones reported here, will eventually create spectral areas of enhanced photooxidation. This effect can be significant for the understanding of photochemical reaction cycles in our atmosphere, or in the atmosphere of planets and moons of our solar system. It indicates that narrow parts of the solar radiation spectrum contribute disproportionately to a photochemical reaction cycle, highlighting the importance of high-resolution terrestrial and space-based solar spectra for the rationalization of VOC budgets.

The effect of ultraviolet radiation in various reactions in the interstellar medium and in planetary objects is a matter of intense research, as for example in the case of water [33]. For the acetylene related reactions, the acetylene highly excited states lie in an area where the solar content rapidly decreases [21], so significant participation of highly excited states should not be expected in the troposphere. However, acetylene is a long-lived compound, with an average lifetime of the order of two months, and is expected to reach the stratosphere [34], where the UV content of the solar spectrum is more substantial.

In addition, as far as acetylene atmospheric reaction cycles are concerned, we note that some of the photooxidation products, such as glyoxal or formaldehyde, which undergo photooxidation as well, have rich absorption spectra in longer wavelengths. Consequently, the excited states of these products are expected to alter the course of their subsequent photooxidation. Apart from acetylene reactions, there is a number of VOCs, such as glyoxylic acid [35], purivic acid [36], as well carbonyl oxides [37], whose atmospheric chemistry is expected to vary significantly upon photoexcitation to specific states. Thus, mapping out the spectral response of such reactions can improve various quantitative predictions related to atmospheric photochemistry.

CRediT authorship contribution statement

Panagiotis Kalaitzis: Software, Investigation, Formal analysis. **Dimitris Sofikitis:** Writing – review & editing, Writing – original draft, Investigation. **Constantine Kosmidis:** Writing – review & editing, Supervision, Resources, Investigation.

Declaration of competing interest

The authors declare that they have no known competing financial interests or personal relationships that could have appeared to influence the work reported in this paper.

Data availability

Data will be made available on request.

Acknowledgments

We acknowledge support of this work by the project “Center for research quality analysis of cultural heritage materials and communication of science (MIS 5047233) which is implemented under the Action “Reinforcement of the Research and Innovation Infrastructure”, funded by the Operational Programme “Competitiveness, Entrepreneurship and Innovation”, Greece (NSRF 2014–2020) and co-financed by Greece and the European Union (European Regional Development Fund).

References

[1] C.Y.R. Wu, T.S. Chien, G.S. Liu, D.L. Judge, J.J. Caldwell, J. Chem. Phys. 91 (1989) 272.
[2] H. Okabe, Can. J. Chem. 61 (1983) 850.
[3] Y. Bénilan, N. Smith, A. Jolly, F. Raulin, Planet. Space Sci. 48 (2000) 463.
[4] B.S. Haynes, H. Jander, H.G. Wagner, Berichte Bunsengesellschaft Phys. Chem. 84 (1980) 585.
[5] J. Hay, R.G.W. Norrish, Proc. R. Soc. London. Ser. A. Math. Phys. Sci. 288 (1965) 17.
[6] S.J. Silva, C.L. Heald, M. Li, J. Geophys. Res.: Atmos. 123 (2018) 13.
[7] C. Lerot, F. Hendrick, M. Van Roozendael, L. Alvarado, A. Richter, I. De Smedt, N. Theys, J. Vlietinck, H. Yu, J. Van Gent, et al., Atmos. Meas. Tech. 14 (2021) 7775.
[8] T.-M. Fu, D.J. Jacob, F. Wittrock, J.P. Burrows, M. Vrekoussis, D.K. Henze, J. Geophys. Res.: Atmos. 113 (2008) D15303.
[9] T. Stevenson, C. Tipper, Combust. Flame 11 (1967) 35.
[10] B.S. Ault, J. Phys. Chem. 93 (1989) 2456.
[11] A.N. Arrowsmith, V. Chikan, S.R. Leone, J. Phys. Chem. A 110 (2006) 7521.
[12] F. Laruelle, S. Boyé-Péronne, D. Gauyacq, J. Liévin, J. Phys. Chem. A 113 (2009) 13210.
[13] E.W.R. Steacie, W.H. Hatcher, J.F. Horwood, J. Chem. Phys. 3 (1935) 291.
[14] E.W.R. Steacie, W.H. Hatcher, J.F. Horwood, J. Chem. Phys. 3 (1935) 551.
[15] L. Zhu, D. Kellis, C.-F. Ding, Chem. Phys. Lett. (ISSN: 0009-2614) 257 (1996) 487.
[16] D.P. Baldwin, M.A. Buntine, D.W. Chandler, J. Chem. Phys. 93 (1990) 6578.
[17] D.H. Mordaunt, M.N. Ashfold, J. Chem. Phys. 101 (1994) 2630.
[18] Y. Zhang, K. Yuan, S. Yu, D.H. Parker, X. Yang, J. Chem. Phys. 133 (2010) 014307.
[19] J. Watson, M. Herman, J. Van Craen, R. Colin, J. Mol. Spectrosc. 95 (1982) 101.
[20] M. Perić, R.J. Buenker, S.D. Peyerimhoff, Mol. Phys. 53 (1984) 1177.
[21] G. Thuillier, P. Zhu, M. Snow, P. Zhang, X. Ye, Light: Sci. Appl. 11 (2022) 1.
[22] N. Shafizadeh, J.-H. Fillion, D. Gauyacq, S. Couris, Phil. Trans. R. Soc. A 355 (1997) 1637.
[23] K. Tsuji, N. Arakawa, A. Kawai, K. Shibuya, J. Phys. Chem. A 106 (2002) 747.
[24] A. Campos, S. Boye, P. Brechignac, S. Douin, C. Fellows, N. Shafizadeh, D. Gauyacq, Chem. Phys. Lett. 314 (1999) 91.
[25] K. Tsuji, K. Misawa, J. Awamura, A. Kawai, K. Shibuya, J. Phys. Chem. A 117 (2013) 1420.
[26] K. Matthíasson, H. Wang, Á. Kvaran, Chem. Phys. Lett. 458 (2008) 58.
[27] A.M. Wodtke, Y. Lee, J. Phys. Chem. 89 (1985) 4744.
[28] B. Balko, J. Zhang, Y.T. Lee, J. Chem. Phys. 94 (1991) 7958.
[29] M.N. Ashfold, G.A. King, D. Murdock, M.G. Nix, T.A. Oliver, A.G. Sage, Phys. Chem. Chem. Phys. 12 (2010) 1218.
[30] K. Matthíasson, H. Wang, Á. Kvaran, Chem. Phys. Lett. 458 (2008) 58.
[31] M.N. Ashfold, R.A. Ingle, T.N. Karsili, J. Zhang, Phys. Chem. Chem. Phys. 21 (2019) 13880.

[32] A. Laufer, R. Lechleider, J. Phys. Chem. 88 (1984) 66.
[33] A. Yabushita, T. Hama, M. Kawasaki, J. Photochem. Photobiol. C: Photochem. Rev. 16 (2013) 46.
[34] M. Kanakidou, B. Bonsang, J. Le Roulley, G. Lambert, D. Martin, G. Sennequier, Nature 333 (1988) 51.
[35] A.W. Harrison, M.F. Shaw, W.J. De Bruyn, J. Phys. Chem. A 123 (2019) 8109.
[36] S.L. Blair, A.E. Reed Harris, B.N. Frandsen, H.G. Kjaergaard, E. Pangui, M. Cazaunau, J.-F. Doussin, V. Vaida, J. Phys. Chem. A 124 (2020) 1240.
[37] T.N. Karsili, B. Marchetti, M.I. Lester, M.N. Ashfold, Photochem. Photobiol. (2022).